IOPscience iopscience.iop.org

Home Search Collections Journals About Contact us My IOPscience

Molecular-dynamics simulations of nucleation and crystallization processes of laser crystallized poly-Si

This article has been downloaded from IOPscience. Please scroll down to see the full text article.

2008 J. Phys.: Condens. Matter 20 055205

(http://iopscience.iop.org/0953-8984/20/5/055205)

View the table of contents for this issue, or go to the journal homepage for more

Download details:
IP Address: 129.252.86.83
The article was downloaded on 29/05/2010 at 08:06

Please note that terms and conditions apply.

J. Phys.: Condens. Matter **20** (2008) 055205 (7pp) doi:10.1088/0953-8984/20/05/055205

Molecular-dynamics simulations of nucleation and crystallization processes of laser crystallized poly-Si

Byoung Min Lee[1,3], Teruaki Motooka[2] and Shinji Munetoh[2]

[1] Department of Materials Engineering, Korea University of Technology and Education, 307, Gajeon-ri, Byeong-chen, Cheon-an Chung-nam 330-708, Korea
[2] Department of Materials Science and Engineering, Kyushu University, 744 Motooka, Nishi-ku, Fukuoka 819-0395, Japan

E-mail: bmlee@kut.ac.kr

Received 2 September 2007, in final form 15 December 2007
Published 14 January 2008
Online at stacks.iop.org/JPhysCM/20/055205

Abstract
The nucleation and crystallization processes of excimer-laser annealed Si on a SiO_2 substrate for complete melting conditions have been investigated by using molecular-dynamics simulations. In the early stage of nucleation, the preferential growth of nuclei with a {111} face normal to the surface was originated from the {111} twin boundaries with a low surface energy. The partial rotation of the dimer leads to the growth of {111}-oriented nuclei along twins that have different stacking sequences. The recombination of vacancies and dimers at the solidification front is directly related to {111} growth from the twin boundaries.

1. Introduction

To realize large-area liquid crystal displays, it is essential to develop a low-temperature fabrication process for high-mobility poly-Si thin-film transistors. Such a process should reduce fabrication costs by allowing the use of low-cost glasses or plastics as a substrate material [1]. SiO_2 glass and quartz play a key role in electronic device applications [2, 3]. It can be expected that the interface energy driven by the structural difference between substrate materials [4] such as quartz and glass influences the stable structure of the Si nucleus at the Si/SiO_2 interface. The interfacial energy of SiO_2 is changed locally by the number of dangling bonds of O and Si atoms at the interface. The difference between the local strain [5] and the interface energy across the interface may lead to the random orientation of grains, as reported in experiments. Among the various crystal growth techniques [6], a widely used method for preparing poly-Si on the glass substrates is excimer-laser annealing (ELA). However, due to the short excimer-laser pulse width, which typically ranges from 20 to 66 ns [7, 8], it is extremely difficult to analyse the nucleation mechanisms of large-grained poly-Si on SiO_2 substrates. Therefore it is desirable to simulate the ELA process on the atomic scale to investigate the conditions leading to a required microstructure, and to understand the effects of various process parameters such as temperature gradient, structure of substrate and cooling rate.

It has been shown that the overall micro-structural trends of Si thin films crystallized on glass substrates by excimer laser can be defined in three major regimes in terms of the applied laser energy density [9]. These are the low-and high-energy-density regimes and, in between these two, the so-called super-lateral growth regime. The high-energy-density regime, where the grain size is nearly independent of the irradiated laser energy density, is related to complete melting of the Si thin film. Hence, this energy range is also referred to as the complete melting regime [10]. Epitaxial growth from the substrates is not possible due to the amorphous structure of the glass. A significant supercooling followed by nucleation in the liquid phase is required before the occurrence of the transformation to the solid phase. The molten Si cools very rapidly ($>10^{10}$ K s^{-1}) [3]. Recent detailed work by Hatano *et al*, who investigated the excimer-laser crystallization process by employing various *in situ* methods, supports the model of homogeneous nucleation in supercooled Si [9]. Up to now, little has been done to investigate the structural development of a grain in laser crystallized poly-Si thin films on the atomic scale.

[3] Author to whom any correspondence should be addressed.

 © 2008 IOP Publishing Ltd Printed in the UK

McCulloch *et al* [11] have investigated the dependence of the hydrogen content on the surface roughening of a Si thin film. The surface roughening mechanism of amorphous a-Si:H is related to the total number of pulses and is independent of the hydrogen content for low hydrogen content, while the hydrogen effect was observed for hydrogen-rich a-Si. Moreover, the surface hydrogen starts to be thermally desorbed at a temperature higher than 400 °C [12]. Since surface Si–H bonds break down over this temperature, the hydrogen in the grain boundary and crystalline Si is expected to be released from the system. Therefore, we assume that there is no large hydrogen effect on the nucleation mechanism at the surface. In this research, molecular-dynamics (MD) simulations of the Si/SiO_2 system have been performed to investigate the nucleation and crystallization processes of Si for the complete melting condition. The structural change of nuclei is thoroughly investigated to understand the preferential {111} growth of the grains normal to the surface.

2. Simulation and model details

The initial MD cell of crystalline silicon (c-Si) was set to $48.9 \times 48.9 \times 97.8$ Å^3. The bottom of the MD cell was cut, and alpha-quartz with a size of $48.9 \times 48.9 \times 30$ Å^3 was inserted. The MD cell contains 7971 atoms for Si and 5687 atoms for SiO_2. To remove the excessive energy at the Si/SiO_2 interface, static structure relaxation was performed. Starting from the idealized interface between the c-Si and the SiO_2 substrate, the condition of complete melting was reproduced by melting the obtained MD cell with an exponential temperature profile up to 20 Å from the interface. The temperatures of the regions below 30 Å and above 50 Å of the MD cell were kept at 1700 and 3500 K, respectively. A melting period of 150 ps was applied to melt the crystalline Si acting as crystal seeds on the SiO_2 substrate. During the cooling process, the temperature of the SiO_2 substrate ($Z \leqslant 30$ Å) was set at 1700 K, and the temperature of the region above 30 Å was not controlled. Periodic boundary conditions were employed in the [100] and [010] directions. In the [001] direction, the atomic positions of two bottom layers of the MD cell were fixed, while an elastic hard wall was set at the top of the MD cell to prevent the atoms from escaping out of the MD cell. The system was divided with a thickness of 5 Å parallel to the surface of the MD cell in order to determine the local temperature change during the cooling process. Approximately 500–600 Si atoms were contained in the region of molten Si. The local temperature of the MD cell was averaged by five different sets of random number. MD simulations were used based on a combination of Langevin and Newton equations to deal with heat transfer from the liquid Si (l-Si) to the SiO_2 substrate [13, 14].

A new parameter set of the Tersoff potential was used to calculate the interatomic forces of Si and O atoms [15]. Since the nucleation of Si was reproduced well by the original Tersoff potential parameter [16], the parameters R_{Si} and S_{Si} that are larger than the original values by 0.2 were used. The short-and intermediate-range orders of SiO_2 were well described by these potential parameters. The structural and dynamical properties of SiO_2, especially regarding the covalent

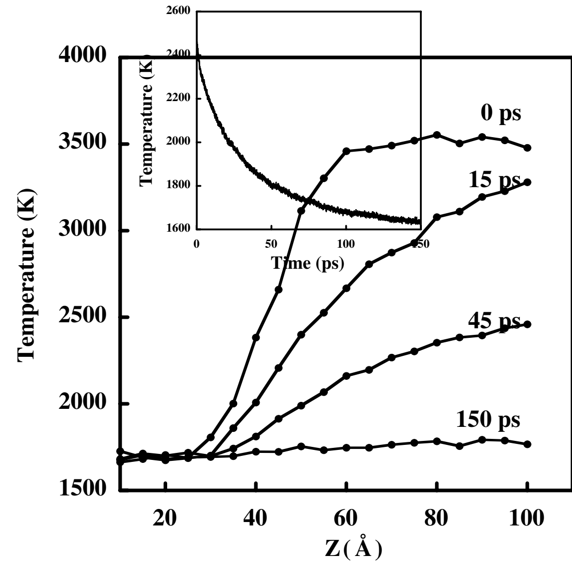

Figure 1. Changes in local temperatures as a function of time during cooling. The temperature of the 30 Å zone of the MD cell is set at 1700 K, and for the other region ($Z > 30$ Å) the temperature was not controlled. The inset shows a time evolution of the overall system temperature during cooling.

characteristics, were in good agreement with the experimental results, even though some discrepancy was observed due to ignorance of the Coulombic interaction. The validity of the new potential parameter set for the Si–O system has also been described in our previous works [17]. In order to control the temperature of the system that was being considered, we used the scheme developed by van Gunsteren and Berendsen for numerical integration of the Langevin equation [18]. The time step for the integration was set at 0.5 fs, and the friction constant was chosen to be 5 ps^{-1}. The Langevin equation for the motion of atom i is:

$$m\ddot{\mathbf{r}}_i(t) = \mathbf{F}_i(t) - m\gamma\dot{\mathbf{r}}_i(t) + \mathbf{R}_i(t), \quad (1)$$

where $\mathbf{F}_i(t)$ is the sum of all forces exerted on atom i by other atoms and is to be derived from the potential which is dependent on the coordinates of all N particles. m is the mass of atoms, γ is the friction constant, and $\mathbf{R}_i(t)$ is a random force to heat the particles. To control overheating, the atoms are subjected to $\mathbf{R}_i(t)$, which simulates the coupling to a heat bath. The detailed simulation procedure is described elsewhere [13, 19].

3. Results and discussion

Figure 1 shows the local temperature change of the system during the cooling process. The local temperatures were averaged by five different sets of random numbers, with a thickness of 5 Å in the [001] direction. The exponential temperature profile at 0 ps was observed near the Si/SiO_2 interface. The temperature of molten Si was decreased and a flattened temperature distribution was obtained in 150 ps. The cooling rate of the l-Si in the natural cooling system depended on the thickness of l-Si and the thermal conductivity

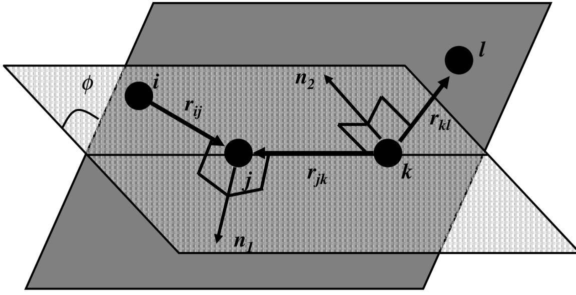

Figure 2. Schematic diagram for the definition of the dihedral angle. The geometry of the atoms is represented in terms of the vectors $\mathbf{r}$, and the dihedral angle can be defined by the angle between vectors $\mathbf{n}_1$ and $\mathbf{n}_2$.

of the substrate material [20], even though a rapid cooling rate of $\sim 10^{13}$ K s^{-1} was obtained in this system. The heat flow from the l-Si to the SiO_2 substrate gives rise to a decrease in the width of the velocity distributions of atoms in the l-Si region [14].

In order to monitor crystal growth and nucleation in l-Si during MD simulations, it is necessary to devise a procedure that allows the identification of crystal-like atoms from liquid-like atoms in an effective way. Marques *et al* [21] reported criteria for discriminating the two phases. In their criteria, all atoms with potential energies 0.2 eV above the ground state of the crystal were identified as amorphous. However, it has been reported that when amorphous material is very well relaxed and in quasi-equilibrium, this criterion leads to error. Uttormark *et al* [22] also proposed a technique for studying the dissolution of crystalline Si embryos in the liquid phase. To identify atoms belonging to the crystalline phase, they used three different criteria based on the coordination of atoms, the distance, and the angles for four nearest neighbors. In this case, nearest neighbors around a central atom form an angle of 109° for the ideal diamond lattice. These three criteria were successfully used for the selection of crystal-like atoms from the liquid environment, since the coordination in the liquid is about 6 [23], and the angles are strongly distorted with respect to those in the perfect crystal lattice.

In this study, the dihedral angle ϕ_{ijkl} shown in figure 2 was used for the definition of the order parameter. The geometry of atoms is represented in terms of the vectors $\mathbf{r}$, and each plane composed of three atoms can be defined by the vectors $\mathbf{n}_1$ and $\mathbf{n}_2$. ϕ_{ijkl} is the angle between the plane containing $\mathbf{r}_{ij}$ and $\mathbf{r}_{ik}$ and that containing $\mathbf{r}_{ik}$ and $\mathbf{r}_{kl}$, where $\mathbf{r}_{ij}$ represents the difference between the position vectors of atoms i and j. The order parameter P_i defined by the dihedral angle can be written as $P_i = 1/(N+1)(\sum_{m=1}^{N} p_m + p_i)$, where $p_i = 1/N_{\phi_{ijkl}} \sum \cos^3(6\phi_{ijkl})$, where p_m is the sum of p_i for the nearest neighbors of atom i, and $N_{\phi_{ijkl}}$ is the number of times calculating ϕ_{ijkl} for atom i. When P_i larger than 0.2, which is the position where the extrapolated point of the density profile and the order parameter profile for each atom meet, an atom is identified as a crystalline atom. By designating crystal atoms as those particles for which $P_i > 0.2$ and liquid atoms as those for which $P_i \leqslant 0.2$, a perfect discriminator is defined.

The atomic configurations identified as crystalline Si atoms and the SiO_2 substrate are shown in figure 3. As can be seen from the figures, crystalline atoms were not observed on the SiO_2 substrate at 0 ps. It is worth noting that homogeneous nucleation in the bulk l-Si and surface nucleation at the top of the MD cell are the significant features for the complete melting condition. The direct formation of nuclei from the SiO_2 substrate was not observed in the simulations. We consider that the high interface energy arising from the lattice mismatch between the SiO_2 substrate and the nuclei leads to the disturbance of nucleation and acts as an activation energy barrier for nucleation at the Si/SiO_2 interface [24].

Figure 4 shows snapshots of the atomic configuration sliced with 5 Å from the top of the MD cell at 22.5 ns and the side view of the atomic configuration of the nucleus formed at the middle region of the surface. The nuclei with {111} facets was observed parallel to the substrate of the MD cell. The preferential orientation of the {111}-oriented faces at the surface is ascribed to the low surface energy [19]. The surface energies for the twinned and untwinned Si surface structures were measured by $\gamma_s = (U_s - U_b)/2A$. Here, U_s is the internal energy of the MD cell with a surface, U_b is the internal energy of bulk Si, and A is the area of the surface. The surface energies of the untwinned Si(111) surface are 1.20 and 1.23 J m^{-2} at 77 and 1700 K, respectively, and the experimental value for the untwinned Si(111) surface is reported to be 1.23 J m^{-2} at 77 K [25]. The surface energies of the twinned Si(111) surface observed in the simulations have the values 1.20 and 1.25 J m^{-2} under the same conditions. The similar values of surface energy for different structures are ascribed to surface atoms with a single dangling bond at twin boundaries and the Si(111) surface, since the surface energy depends on the dangling bond density at the surface. The effect of the surface energy for nucleation can be associated with classical nucleation theory. Nucleation and crystal growth is possible at a smaller critical nucleus size with decreasing surface energy. Twin boundaries are the dominant microstructure in a preferential {111} orientation of grains, and the predominant formation of twin boundaries is a general feature of the grains [26].

As shown in figure 4(b), the structure of the first monolayer from the surface represents twins, and the twin boundaries are parallel to the surface of the MD cell. The twins or stacking faults are expected to form {111} faces for the reduction of stresses and nucleation sites for easier growth, and grow along the {111} faces once they have formed [27]. Therefore, the dominant evolution of {111} faces at the surface can be thought to be a consequence of the low surface energy, and the twinned crystals act as a preferential growth site compared to a structure without twinning [28]. Christiansen *et al* reported that the grains in laser crystallized poly-Si were dominated by first-and second-order twin boundaries and, under certain experimental conditions, preferential {111} grains normal to the surface could be obtained [26]. More confident evidence of growth with {111}-oriented surfaces from the twin boundaries is observed in the preferential growth of the flattened diamond crystal, arising from the twin re-entrant corner effect [29].

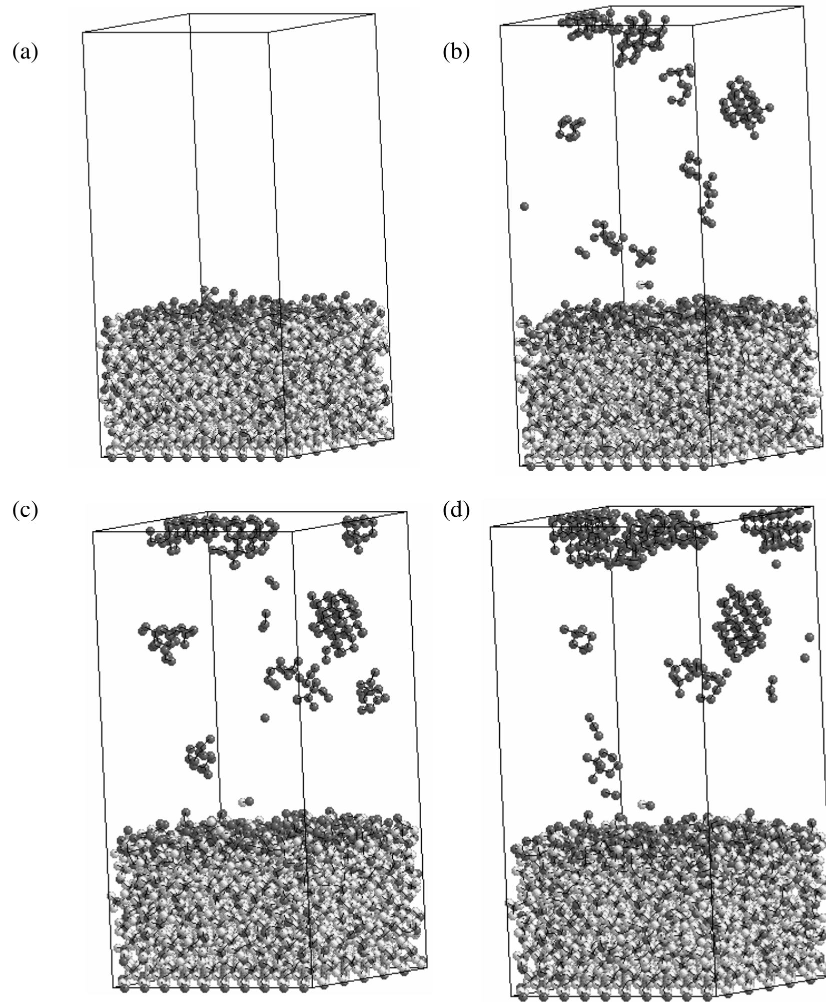

Figure 3. Snapshots of atomic configuration during nucleation and crystallization processes: (a) $t = 0.0$ ns, (b) $t = 15$ ns, (c) $t = 18$ ns, and (d) $t = 22.5$ ns. These snapshots were obtained by projecting the atomic configurations identified as the c-Si atoms and the SiO_2 substrate. The O and Si atoms are represented by white and dark gray, respectively.

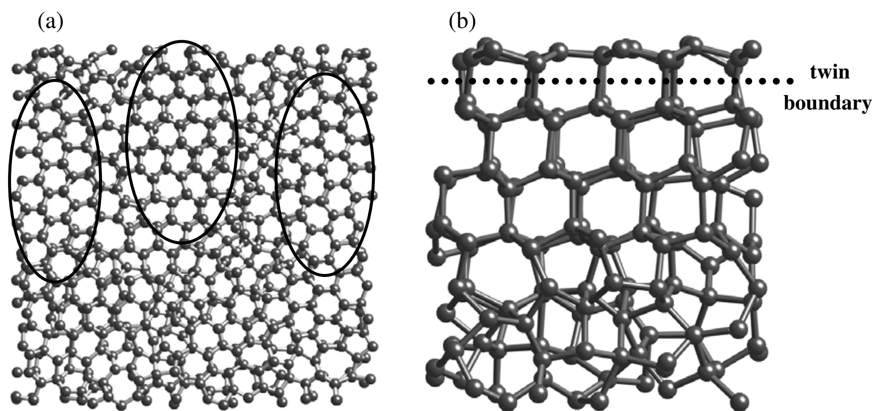

Figure 4. Snapshots of atomic configuration for the surface atoms at 22.5 ns. Encircled regions indicate nuclei with {111} faces. The atomic positions are projected on the [001] direction for the top 5 Å-thick region of the MD cell (a). The atomic configuration of (b) is projected along the high-symmetry direction of the nucleus. The dotted line indicates the twin boundary.

To obtain more details on the surface structure, we investigated the micro-structural evolution of several structures during the phase transformation with time. It should be noted that the probability of observing crystal growth from the defects in an MD cell containing 8000 Si atoms is very low due to the difficulty of defect formation in the Tersoff potential [30]. Even though five- and seven-member rings near the perfect c-Si are frequently observed in the solid/liquid

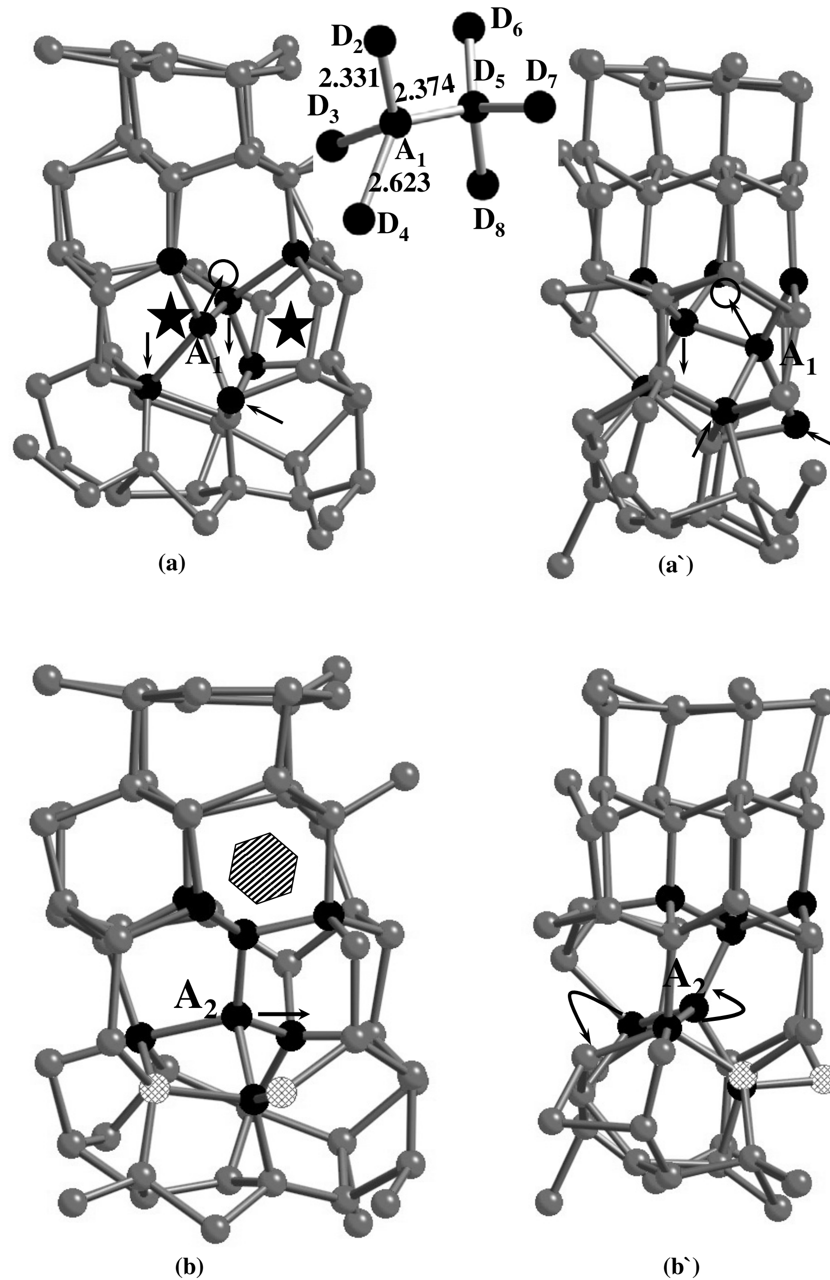

Figure 5. Observed formation processes of the {111} face from the twin boundaries: (a) $t = 21.526$, (b) $t = 21.535$, (c) $t = 21.55$, and (d) $t = 21.64$ ns. The hollow hatched atoms and the atoms pointed out by arrows indicate the atoms participating in the growth of the {111} face from the twin boundaries. The vacant sites and the five- and seven-member rings at the solidification front are indicated by a circle and a black star, respectively. The atomic configurations of the nucleus are projected along the high-symmetry direction of the nucleus. The black atoms indicate the dimer.

interface, crystal growth of Si(111) from the twin layer has not been reported. Figure 5 shows a typical example of the atomic arrangement corresponding to a crystallization event by interchanging the positions indicated by the small arrows and the schematic sequence of formation of the {111} face from the twin boundaries. The migration and transformation processes of atoms through several paths have been identified by careful analysis of the computer-generated trajectories. Two different views of the solidification front along high-symmetry directions of the nucleus are shown for each step. Five- and seven-member rings formed around the dimer are indicated by the black stars in figures 5(a) and (c). It is seen that the dimer created in front of the twinned Si layer performs a partial rotation and ends up in crystalline positions. The feature of the dimer observed at 21.562 ns is that the internal angles formed by $\angle D_6D_5D_7$, $\angle D_7D_5D_8$ and $\angle A_1D_5D_8$ are 116.7°, 112.1°, and 105.5°, respectively. These are in the range 105°–117°. The lengths of bonds involved in the dimer were estimated to be, respectively, 2.374, 2.331, and 2.623 Å for A_1–D_5, A_1–D_2 and A_1–D_4, which are in good agreement with those calculated by Cargnoni *et al* [31] when the reaction path coordinate was 0.09. The bond lengths and bond angles between the first-

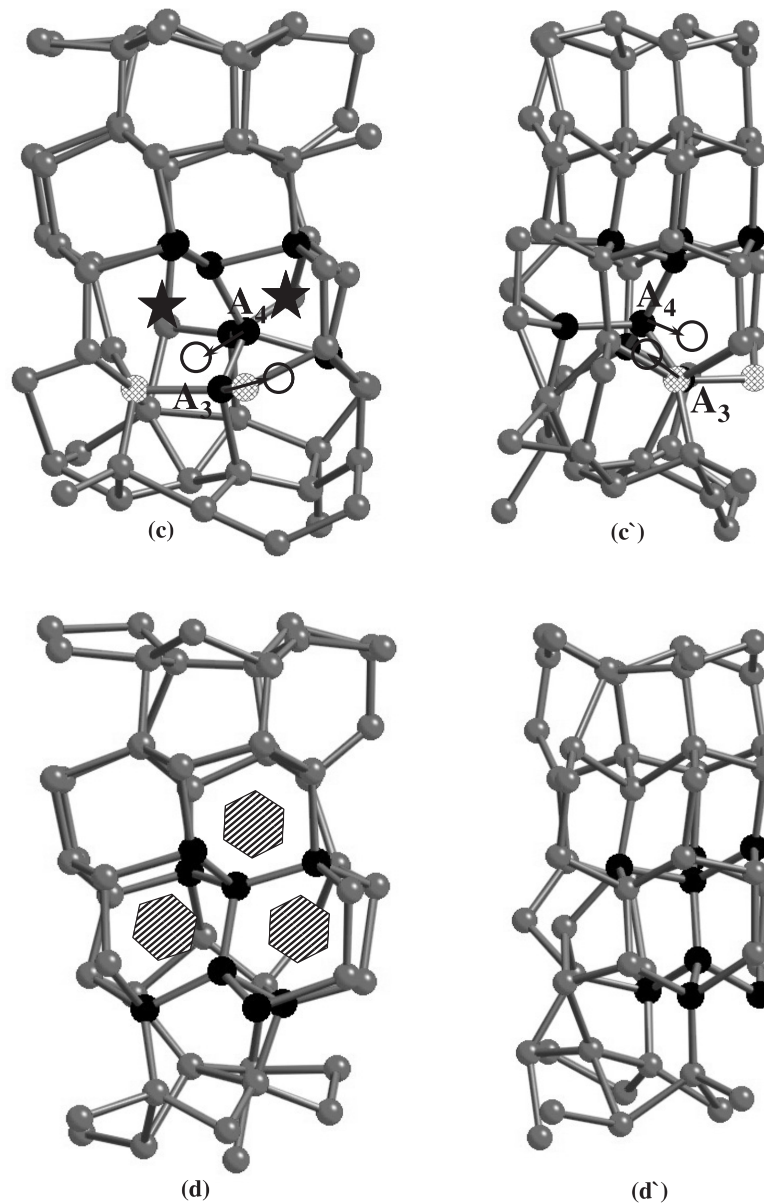

Figure 5. (Continued.)

nearest-neighbor atoms of the dimer shown in figure 5(a) were confirmed to be almost equal to those of c-Si (the atomic distance is 2.352 Å, and the bond angle is 109.471° at 0 K), and almost all of these atoms are fourfolded.

The A_1 dumbbell atom migrates to the vacant site which the dumbbell atoms consisting of five- and seven-member rings shared before recombination (figure 5(a)), resulting in the formation of a six-member ring (figure 5(b)). The A_2 atom is pushed in the direction indicated by the arrows and induces a local distortion around the dimer. In this migration process, new five- and seven-member rings and the vacant sites around the dimer were created (figure 5(c)). Finally, the A_3 and A_4 atoms are located near to the vacant sites. The A_4 dumbbell atom is pulled toward the vacancy, and the A_3 and A_4 atoms form two six-member rings by new bonds with the hollow hatched atoms that are originally included in the dimer, as shown in figure 5(a). The described formation process gives the structural rearrangement that takes place between the {111} faces and the twin boundaries by the spontaneous recombination of the vacancy and dimer atoms generated by five- and seven-member rings. The spontaneous recombination process, resulting in the crystallization of a {111} face from the twin boundaries, is similar to the interstitial–vacancy complex that was observed in the MD simulations by Marques [32] and Tang *et al* [33]. In their simulations, the recombination process for artificially generated interstitial and vacancy pairs occurred in the c-Si matrix. Comparison between the initial and final steps makes clear the changes in bonding at the solidification front due to a small torsion around the dimer and the local diffusion of atoms, resulting in the formation of two six-member rings marked by the hatched hexagons in figure 5(d). Since the atoms in the (111) plane need just

one bond for further growth perpendicular to the surface, a local movement of atoms included in the dimer leads to the preferential growth of an atomic layer along the (111) plane that has a different stacking sequence from the c-Si (twin boundaries) at the surface. In addition, vacancy and dimer formation at the solidification front is directly related to the growth of the {111} face from the twin boundaries.

4. Conclusions

In conclusion, we have performed MD simulations for the analysis of nucleation and crystallization processes of poly-Si on a SiO_2 substrate for complete melting. The nucleus nucleated at the surface had {111} faces normal to the surface. It was observed that the crystallization mechanism of the {111} face nucleated at the surface was involved in the twin-dominated defect structure, and the interactions of vacancies and dimers generated at the solidification front leads to the formation of the {111} face from the twin boundaries. Since the preferential growth of the elongated and flattened {111}-oriented surface was related to crystal growth from twin boundaries parallel to the surface, the simulation results suggest that the {111}-oriented nuclei at the surface can be derived from the twin boundaries that have a low surface energy.

Acknowledgments

This work was partly supported by the Japanese Ministry of Economy, Trade and Industry, by the New Energy and Industrial Technology Development Organization, and by the Advanced LCD Technologies Development Center Co. Ltd.

References

[1] Do-Young K, Myung-Suk S, Chi-Hyung K and Junsin Y 2004 *Thin Solid Films* **453/454** 100
[2] Tsunoda I, Matsuura R, Tanaka M, Watakabe H, Sameshine T and Miyao M 2006 *Thin Solid Films* **508** 96
[3] Sameshima T and Usui S 1993 *J. Appl. Phys.* **74** 6592
[4] Atwater H A, Thompson C V and Smith H I 1988 *J. Mater. Res.* **3** 1232
[5] Pasquarello A, Hybertsen M S and Car R 1996 *Appl. Phys. Lett.* **68** 625
[6] Ebiko Y, Suzuki K and Sasaki N 2005 *IEEE Trans. Electron Devices* **52** 429
[7] Ishihara R, Burtsev A and Alekemade F A 2000 *Japan. J. Appl. Phys.* **39** 3872
[8] Sposili R S and Im J S 1996 *Appl. Phys. Lett.* **69** 2864
[9] Hatano M, Moon S and Lee M 2000 *J. Appl. Phys.* **87** 36
[10] Im J S and Kim H J 1994 *Appl. Phys. Lett.* **64** 2303
[11] McCulloch D J and Brotherton S D 1995 *Appl. Phys. Lett.* **66** 2060
[12] Hamakawa Y 2004 *Thin-film Solar Cells: Next Generation Photovoltaics and its Applications* (New York: Springer) p 74
[13] Lee B M, Seong B S, Munetoh S and Motooka T 2006 *J. Korean Phys. Soc.* **49** 2353
[14] Lee B M, Munetoh S and Motooka T 2006 *Comput. Mater. Sci.* **37** 198
[15] Munetoh S, Motooka T, Moriguchi K and Shintani A 2007 *Comput. Mater. Sci.* **39** 334
[16] Motooka T and Munetoh S 2004 *Phys. Rev.* B **69** 073307
[17] Lee B M, Seong B S, Baik H K, Munetoh S and Motooka T 2006 *Comput. Mater. Sci.* **37** 203
[18] Gunsteren W F and Nerendsen H J C 1982 *Mol. Phys.* **45** 637
[19] Lee B M, Kuranaga T, Munetoh S and Motooka T 2007 *J. Appl. Phys.* **101** 054316
[20] Lee B M, B S Seong, Baik H K, Munetoh S and Motooka T 2007 *Amorphous and Polycrystalline Thin-Film Silicon Science and Technology* (*Mater. Res. Soc. Symp. Proc.* 910) ed S Wagner, V Chu, H A Atwater, K Yamamoto and H-W Zan (Warrendale, PA: Materials Research Society) p A05-05
[21] Marques L A, Caturla M J, Diaz Tomas, de la Rubia and Gilmer G H 1996 *J. Appl. Phys.* **80** 6160
[22] Uttormark J, Thompson M O and Clancy P 1993 *Phys. Rev.* B **47** 15717
[23] Cook S J and Clancy P 1993 *Phys. Rev.* B **47** 7686
[24] Tu Y and Tersoff J 2000 *Phys. Rev. Lett.* **84** 4393
[25] Jaccodine R J 1963 *J. Electrochem. Soc.* **110** 524
[26] Christiansen S, Lengsfeld P, Krinke J, Nerding M, Nickel N H and Strunk H P 2001 *J. Appl. Phys.* **89** 5348
[27] Furukawa S 1985 *Silicon on Insulator: its Technology and Application* (Tokyo: KTK Scientific Publishers) p 63
[28] Ming N and Sunagawa I 1988 *J. Cryst. Growth* **87** 13
[29] Hirabayashi K, Kimura T and Hirose Y 1993 *Appl. Phys. Lett.* **62** 354
[30] Ungar P J, Halicioglu T and Tiller W A 1994 *Phys. Rev.* B **50** 7344
[31] Cargnoni F, Gatti C and Colombo L 1998 *Phys. Rev.* B **57** 170
[32] Marque L A, Pelaz L, Hernandez J and Barbolla J 2001 *Phys. Rev.* B **64** 045214
[33] Tang M, Colombo L, Zhu J and de la Rubia T D 1997 *Phys. Rev.* B **55** 14279